npj | regenerative medicine

Article

Published in partnership with the Australian Regenerative Medicine Institute

https://doi.org/10.1038/s41536-024-00388-6

Macrophage-derived extracellular vesicles transfer mitochondria to adipocytes and promote adipocyte–myofibroblast transition in epidural fibrosis

Feng Hua[1,3], Jinpeng Sun[1,3], Mohan Shi[1], Rui Mei[1], Zeyuan Song[1], Jun Liu[1] ✉ & Mingshun Zhang[2] ✉

Epidural fibrosis post laminectomy is the leading cause of failed back surgery syndrome. Little is known about the role and mechanisms of adipose tissues in epidural fibrosis. Here, we found that obese patients were more likely to develop epidural fibrosis after spine surgery. Similarly, obesity led to more progressive epidural fibrosis in a mouse model of laminectomy. Adipocyte–myofibroblast transition (AMT) occurs in epidural scarring. Mechanistically, large extracellular vesicles (EVs) from M2-type macrophages transfer mitochondria into adipocytes and promote AMT by activating the TGF-β and PAI-1 pathways. Blocking the PAI-1 pathway significantly attenuated the transition of adipocytes into myofibroblasts. We conclude that large EVs from macrophages transfer mitochondria to promote AMT in epidural fibrosis.

With the aging of society, more people are suffering from degenerative diseases of the lumbar spine, in which the nerves and spinal cord are compressed, even leading to paralysis[1]. In this context, laminectomy, a surgery designed to relieve compression, is increasingly used[2]. However, some patients may develop failed back surgery syndrome (FBSS) following spine operation[3]. One of the leading causes of FBSS is massive epidural fibrosis[4]. The specific mechanisms of epidural fibrosis are still largely unknown.

Obesity, a modern pandemic, is an independent risk factor for spine degeneration[5]. Adipose tissues store excess energy in the form of triglycerides in lipid droplets[6]. In addition, adipose tissues provide mechanical cushioning in certain areas, such as the buttocks, heels and epidural areas[7]. Epidural fat is located mainly on the dorsal side of the epidural space and is present in the thoracic and lumbar spine[8]. In epidural fat, adipocytes constitute the majority[9]. Adipocytes have been found to regulate metabolism and influence inflammation[10], but their role in tissue repair and epidural fibrosis remains unclear. Adipocytes may serve as a source of myofibroblasts and thus participate in the development of fibrosis[11], especially in dermal-related diseases[12–14]. In this study, we found that epidural adipocytes transform into myofibroblasts, which secrete extracellular matrix and promote epidural fibrosis after laminectomy.

Macrophages, known as one of the most common types of innate immune cells, are involved in many physiological processes[15]. It is generally accepted that macrophages can be divided into M1-type and M2-type macrophages, with M1 macrophages being the main type involved in the inflammatory response and M2 macrophages being the main type involved in tissue repair[16]. In our study, we found that macrophages migrated around epidural adipocytes after laminectomy. Moreover, macrophages, especially M2-type macrophages, promote the conversion of adipocytes into myofibroblasts. This process is regulated by extracellular vehicles (EVs) derived from macrophages. EVs are small vesicle-like bodies with a double membrane structure ranging from 40 nm to 1000 nm in diameter[17]. EVs act as transport vehicles, carrying biological molecules such as RNA, proteins, carbohydrates and lipids[18]. Recent studies have shown that extracellular vesicles may also carry mitochondria, which regulate cell metabolism and function when they enter cells[19]. As bilayer organelles that exist in most eukaryotic cells, mitochondria are the main sites of aerobic respiration and oxidative phosphorylation and provide energy for cellular activities[20]. In addition to providing energy, mitochondria are involved in many processes,

[1]Department of Orthopedics, The Second Affiliated Hospital of Nanjing Medical University, Nanjing, China. [2]NHC Key Laboratory of Antibody Technique, Jiangsu Province Engineering Research Center of Antibody Drug, Department of Immunology, Nanjing Medical University, Nanjing, China. [3]These authors contributed equally: Feng Hua, Jinpeng Sun. ✉e-mail: 13776698080@139.com; mingshunzhang@njmu.edu.cn

i.e., cell differentiation[21]. Here, we show that mitochondria from large EVs derived from M2 macrophages fuel the trans-differentiation of adipocytes into myofibroblasts in epidural fibrosis.

Results

Effects of obesity on postoperative epidural fibrosis

To explore whether obesity played a role in the development of the epidural scar, we obtained the Oswestry disability index (ODI) from patients before laminectomy and one year after surgery. Then, we subtracted the preoperative ODI from the postoperative ODI to obtain the ΔODI, and a higher ΔODI indicated greater back pain relief and a better prognosis. The results revealed that obese patients tended to have a worse prognosis (Fig. 1A, B). After scoring the epidural scars in the MR images of the patients, we concluded that obese patients tended to produce more epidural scars than normal weight patients (Fig. 1C, D).

To further dissect the role of obesity in epidural fibrosis, we performed laminectomy in OB/OB (leptin$^{-/-}$) mice. The expression of fibronectin, α-SMA and collagen 1 in epidural scar tissues was greater in OB/OB mice than in wild-type mice 30 days after laminectomy (Fig. 2A, B). In the epidural area, we observed increased expression of α-SMA in OB/OB mice 30 days after laminectomy (Fig. 2C). In addition, more inflammatory infiltration (Fig. 2D) and collagen deposition (Fig. 2E) were observed in the OB/OB mice than in the wild-type mice after surgery. Clinically, a large proportion of patients are obese because of poor diet control. Therefore, to better simulate the clinical situation, we obtained obese mice that were fed with a high-fat diet (HFD). As expected, the HFD promoted epidural fibrosis (Supplementary Fig. 1). Collectively, these data suggest that obesity is positively linked to epidural fibrosis after spine surgery.

Adipocytes are involved in epidural scar formation

To further investigate the mechanisms of obesity in epidural fibrosis, we collected patients' epidural scar tissues and scar-adjacent tissues for proteomics. We found that the ACSL1 and DGAT1 proteins were highly expressed in the epidural scar (Fig. 3A). Both ACSL1 and DGAT1 can regulate the formation of triglycerides and affect the metabolism and function of adipocytes[22,23]. GO analysis revealed that neutral lipid metabolic processes and fatty acid metabolic processes were involved in the formation of epidural scars (Fig. 3B). KEGG analysis revealed that the PPAR signaling pathway[24], which plays an important role in regulating the formation and function of adipocytes, is involved in the formation of epidural scars (Fig. 3C). We detected that ACSL1 and DGAT1 were indeed highly expressed in scar tissues from patients (Fig. 3D). We obtained adipose tissue from patients who underwent laminectomy or patients who required sacrectomy due to epidural scar hyperplasia. The adipose tissues from the revision surgery group showed more inflammatory infiltration and a greater change in the morphology of the adipocytes (Fig. 3E). TGF-β is a master cytokine for fibrosis. In response to treatment with TGF-β, the number of lipid droplets in adipocytes begins to decrease (Supplementary Fig. 2a). A portion of adipocytes stimulated with TGF-β expressed the myofibroblast marker α-SMA (Supplementary Fig. 2b, c). The levels of fibronectin and α-SMA were increased, while the expression of PLIN-1 was decreased after stimulation with TGF-β (Supplementary Fig. 2d). Indeed, we found that the adipocyte marker PLIN1 and the myofibroblast marker α-SMA were highly colocalized in adipose tissues from revision surgery patients (Fig. 3F), indicating that adipocytes may transdifferentiate into myofibroblasts.

Macrophages regulate the adipocyte–myofibroblast transition

We observed that the morphology of epidural adipocytes in obese mice changed significantly (Fig. 4A). The number of cells that expressed both PLIN-1 and α-SMA in obese mice increased over time after laminectomy (Fig. 4B). Representative images 30 days after surgery revealed the same trend, with more adipocytes expressing the α-SMA protein (Fig. 4C). As an important component of adipose tissues[25], macrophages have been found to affect the function of adipocytes[26]. The macrophages infiltrated around adipocytes in the obese mice 30 days after laminectomy (Fig. 4D). The enlarged images revealed that the adipocytes near the macrophages were

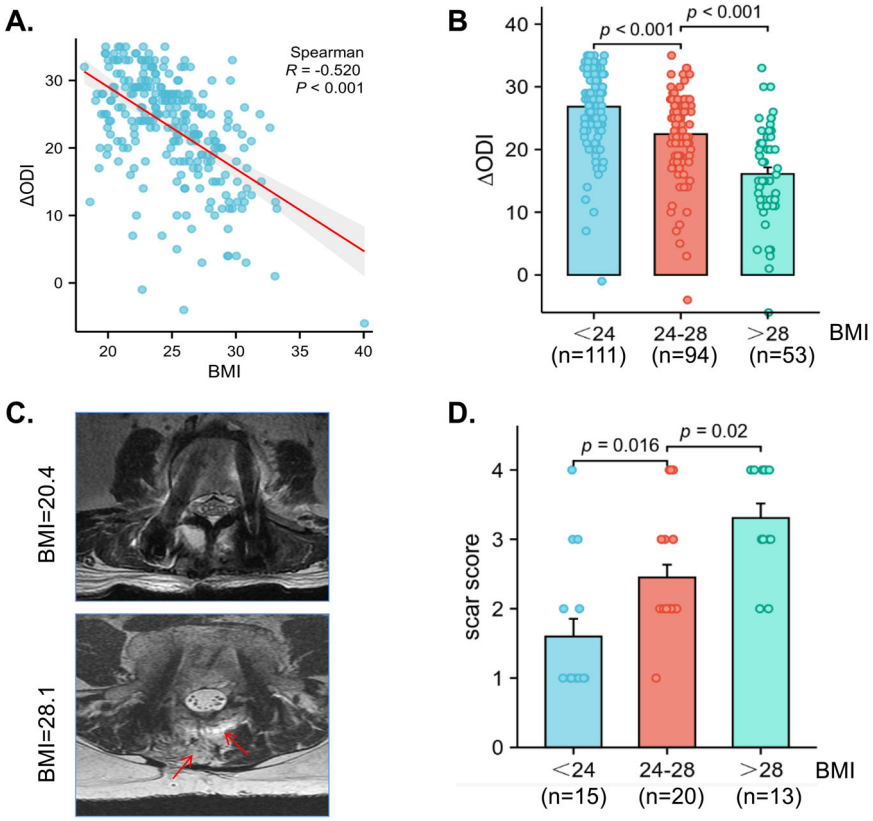

Fig. 1 | Postoperative back pain and scar hyperplasia are associated with obesity. A The correlation scatter plot shows that BMI was negatively correlated with the ΔODI. ΔODI equals the postoperative ODI minus the preoperative ODI. **B** The patients were divided into three groups according to their BMI, and the results revealed that the ΔODI was lowest in the group whose BMI was higher than 28 kg/m^2 and highest in the group whose BMI was lower than 24 kg/m^2. **C** Patients were subjected to MRI examination 1 year post spine operation. Typical MR images of patients with different BMIs 1 year after surgery. The obese patients had more epidural fibrosis than did the patients with a normal BMI. Arrows indicated the areas of fibrosis. **D** The patients were divided into three groups according to their BMI, and the results revealed that the scar score was highest in the group whose BMI was higher than 28 kg/m^2 and lowest in the group whose BMI was fewer than 24 kg/m^2. Values are mean ± SEM.

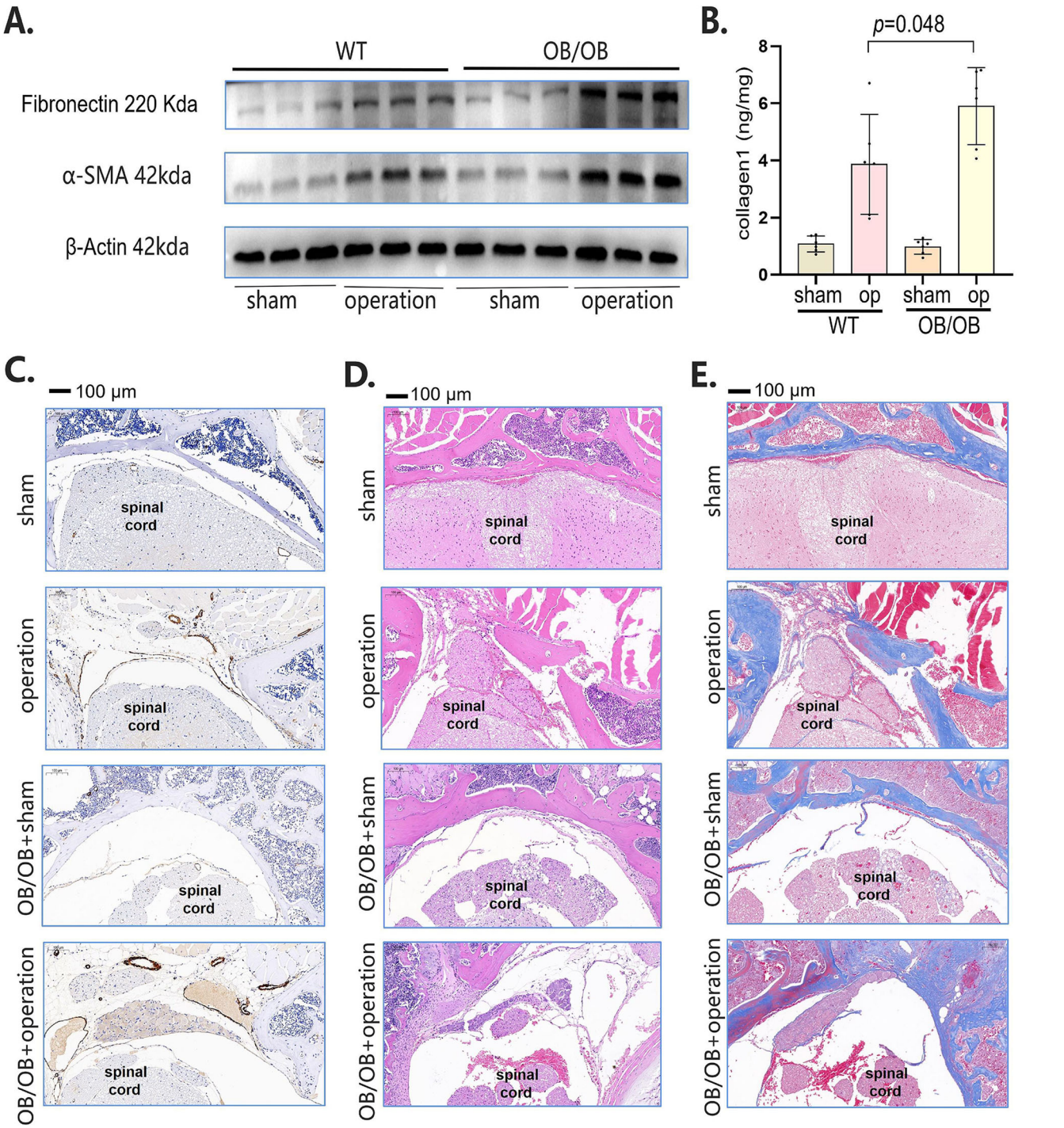

Fig. 2 | OB/OB mice developed more epidural fibrosis. A Western blot analysis of fibronectin and α-SMA in OB/OB mice and normal control mice subjected to sham surgery or laminectomy. **B** ELISA analysis of collagen-1 in OB/OB mice and normal control mice subjected to sham surgery or laminectomy. **C** Immunohistochemical staining of α-SMA (brown) in OB/OB mice and normal control mice subjected to sham surgery or laminectomy. **D** HE staining of OB/OB mice and normal control mice subjected to sham surgery or laminectomy. **E** Masson staining of OB/OB mice and normal control mice subjected to sham surgery or laminectomy. Values are mean ± SEM.

deformed, whereas the adipocytes far from the macrophages remained unchanged (Fig. 4D). To confirm the roles of macrophages in adipocytes, we used liposomes encapsulating clodronate, a well-established method for the macrophage depletion[27]. In our previous publication, we utilized clodronate liposomes to deplete macrophages and achieved an elimination rate exceeding 80%[1,28]. Once macrophages were depleted, the percentage of AMT decreased (Fig. 4E, F), suggesting that macrophages regulate AMT during epidural fibrosis.

M2 macrophage-derived large vesicles promoted AMT

To investigate whether macrophages promote AMT and the specific mechanisms involved, we cocultured macrophages and adipocytes in a Transwell system. We placed macrophages in the upper compartment of the insert chamber and found that the lower adipocytes developed different levels of AMT. Compared with M1-type macrophages, M2-type macrophages had greater potential to promote AMT (Fig. 5A). Macrophages may release extracellular vesicles and communicate with other cells[29]. Therefore,

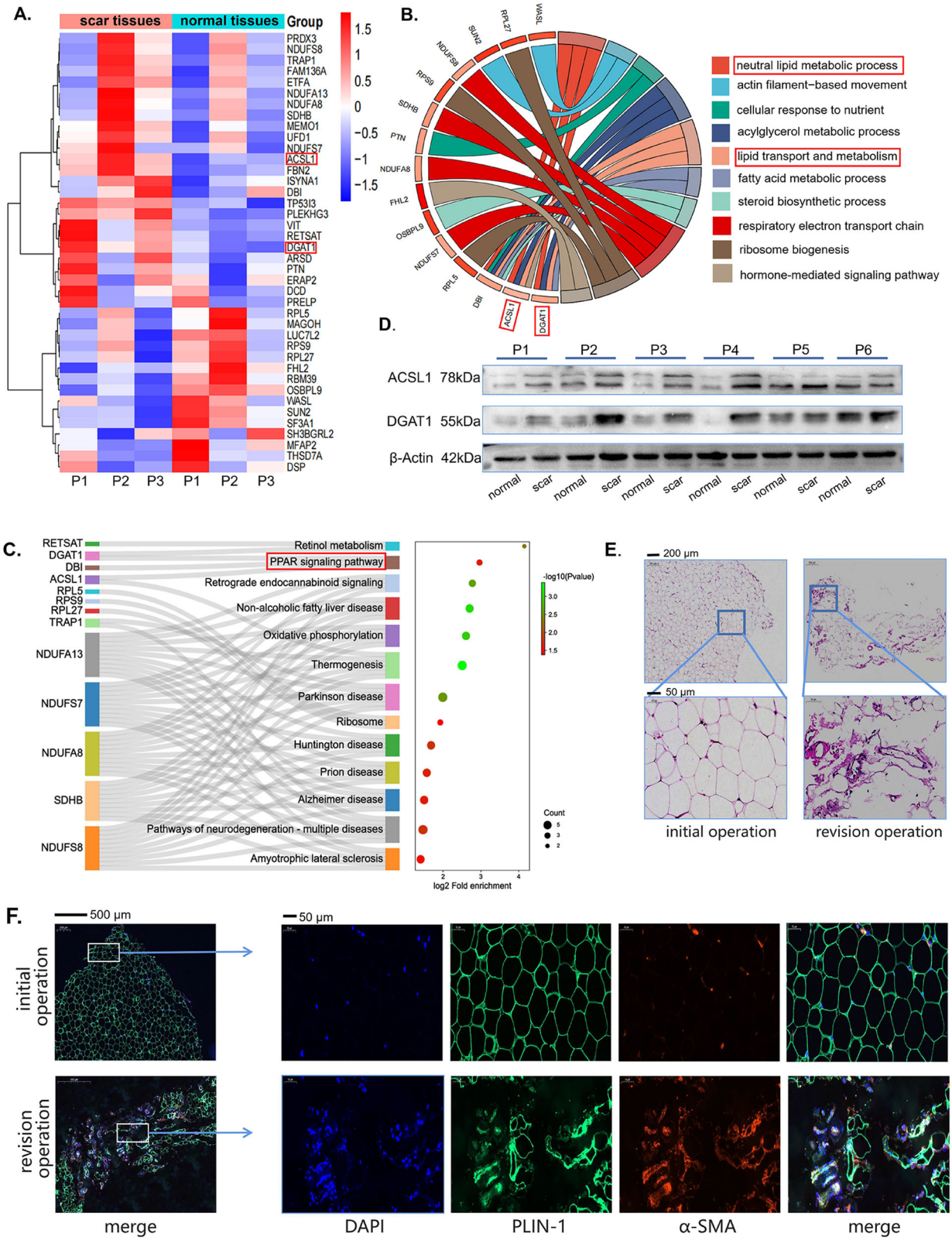

Fig. 3 | Adipocytes are involved in the development of epidural fibrosis. **A** Proteomic analysis was conducted on the scar tissue and normal tissue from three patients. Proteins with a fold change greater than 1.2 or less than 0.8, and a *p* value less than 0.05, were identified as differentially expressed proteins. The results were presented in the form of a heatmap. **B** Differential proteins from the scar tissue and normal tissue of three patients were subjected to Gene Ontology (GO) enrichment analysis. **C** Differential proteins from the scar tissue and normal tissue of three patients were subjected to KEGG enrichment analysis. **D** Western blot analysis of DGAT1 and ACSL1 in scar and normal tissues from patients. **E** HE staining of adipose tissues from patients who underwent primary surgery or revision surgery. **F** Immunofluorescence staining of PLIN1 (pseudogreen) and α-SMA (pseudored red) in adipose tissues from patients who underwent primary surgery or revision surgery.

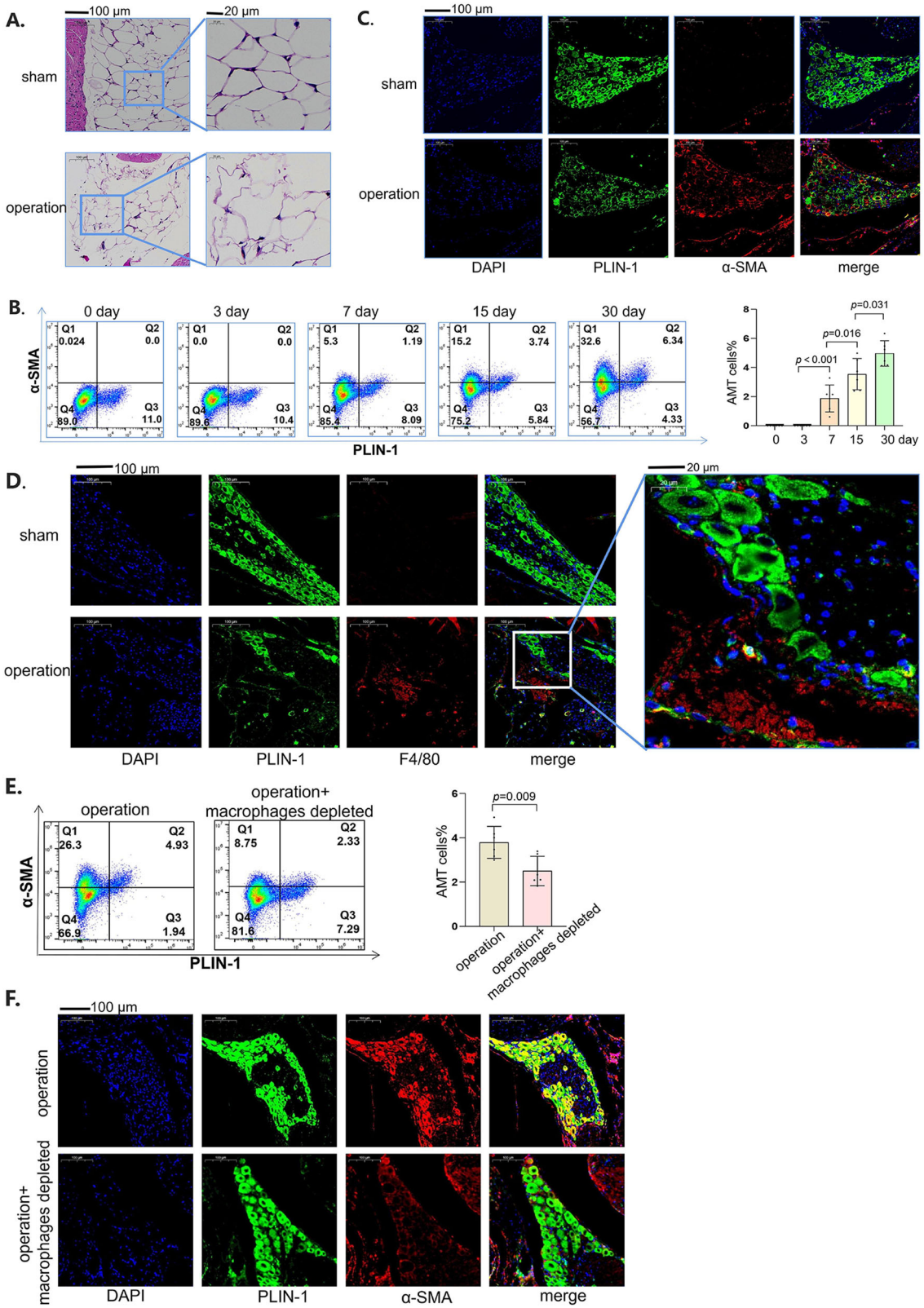

Fig. 4 | Macrophages promoted the adipocyte–myofibroblast transition. A HE staining of epidural adipose tissues from obese mice 30 days after laminectomy or without laminectomy. **B** PLIN1 and α-SMA expression in obese mice at different times after laminectomy was detected via flow cytometry. On the left are typical images of flow cytometry, and on the right is the statistical graph after the experiment was repeated six times. **C** Immunofluorescence of PLIN1 (pseudogreen) and α-SMA (pseudocolored red) in obese mice 30 days after surgery or sham surgery. **D** Immunofluorescence of PLIN1 (pseudogreen) and F4/80 (pseudored red) in obese mice 30 days after surgery or sham operation. **E** PLIN1 and α-SMA expression in obese mice was detected by flow cytometry. On the left are typical images of flow cytometry, and on the right is the statistical graph after the experiment was repeated six times. **F** Immunofluorescence of PLIN1 (pseudogreen) and α-SMA (pseudored) in obese mice 30 days after surgery. Values are mean ± SEM.

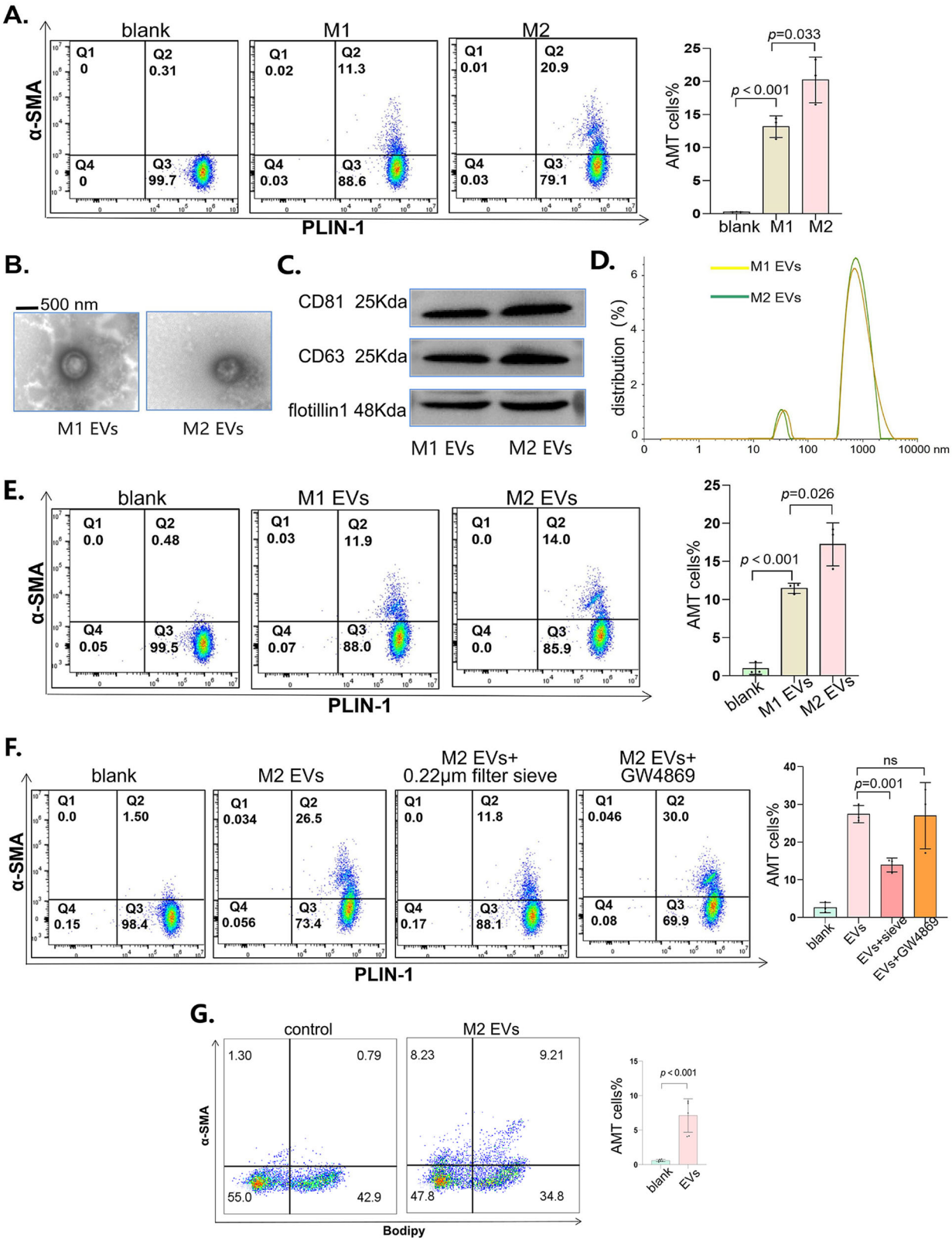

we extracted vesicles from the supernatant of M1-type or M2-type macrophages and observed the morphology of the vesicles (Fig. 5B). Additionally, we detected the markers CD81, CD63, and flotillin to identify the vesicles (Fig. 5C). The diameter of the vesicles was mostly between 500 and 1500 nm, and a small number of the vesicles were less than 100 nm in diameter (Fig. 5D). We used macrophage-derived vesicles to stimulate adipocytes. The results showed that M2-derived vesicles promoted AMT more than did M1-derived vesicles (Fig. 5E). To determine whether exosomes less than 100 nm in diameter or vesicles larger than 500 nm play a role in AMT, we used a 0.22 μm sieve to filter large-diameter vesicles and showed that AMT was significantly inhibited. Moreover, we used GW4869 to inhibit the release of small-diameter vesicles[30], and AMT was not inhibited (Fig. 5F).

Fig. 5 | M2 macrophage-derived large vesicles promoted AMT. A PLIN1 and α-SMA expression in adipocytes cocultured with M1- or M2-type macrophages was detected via flow cytometry. On the left are typical images of flow cytometry, and on the right is the statistical graph after the experiment was repeated three times. **B** Typical images of extracellular vesicles observed via transmission electron microscopy. **C** Western blot analysis of CD81, CD63 and flotillin-1 in vesicles derived from M1 or M2 macrophages. **D** The diameter of the vesicles was measured via NTA. **E** PLIN1 and α-SMA in adipocytes treated with vesicles derived from M1- or M2-type macrophages were detected via flow cytometry. On the left are typical images of flow cytometry, and on the right is the statistical graph after the experiment was repeated three times. **F** Before we stimulated adipocytes with vesicles, we filtered the extracted vesicles with a 0.22 μm sieve or treated macrophages with CCCP prior to vesicle extraction. Then, we detected PLIN1 and α-SMA in adipocytes via flow cytometry. On the left are typical images of flow cytometry, and on the right is the statistical graph after the experiment was repeated three times. **G** Flow cytometry was used to detect lipid content (BODIPY staining) and the expression of α-SMA in adipose tissue. On the left are typical images of flow cytometry, and on the right is the statistical graph after the experiment was repeated six times. All the data are presented as the mean ± Standard Error of the Mean (SEM).

To assess whether the vesicles derived from macrophages have the desired efficacy in vivo, we injected the vesicles into the adipose tissue of the inguinal region in mice and subsequently employed flow cytometry to detect the occurrence of AMT. The adoptive transfer of EVs indeed increased the expression of α-SMA in adipocytes (Fig. 5G). Overall, we concluded that large vesicles from macrophages may promote AMT.

Large vesicles transmitted mitochondria to induce AMT

When we stimulated adipocytes with macrophage-derived vesicles, the expression of mitochondria-related proteins increased in adipocytes (Fig. 6A). To explain this phenomenon, we suspected that the vesicles contained mitochondria and carried them into adipocytes. Therefore, we used MitoTracker staining to label the mitochondria in the vesicles, and the results revealed that the vesicles contained mitochondria and that the M2-derived vesicles contained more mitochondria than did the M1-derived vesicles (Fig. 6B). Similarly, we found that M2-derived vesicles contained more mitochondria-related proteins than M1-derived vesicles (Fig. 6C). Moreover, we observed that in M2-type macrophages, vesicles were secreted from the mitochondria, which indicated that the vesicles could contain the components of the mitochondria (Fig. 6D). To confirm that macrophages can transfer mitochondria to adipocytes, we stained macrophages with MitoTracker and cocultured them with adipocytes via a Transwell system. After 24 h of coculture, the proportion of adipocytes positive for MitoTracker staining was measured. The results showed that M2-type macrophages could transfer more mitochondria to adipocytes than M1-type macrophages (Fig. 6E). When we used a 0.22 μm sieve to remove large EVs, we found that the number of transferred mitochondria was significantly reduced, indicating that large vesicles may dominate mitochondrial transport (Fig. 6F). To study whether vesicle-transported mitochondria were indispensable to AMT, we inhibited mitochondrial function in macrophages with CCCP, a mitochondrial oxidative phosphorylation uncoupling agent[31]. When vesicles with inhibited mitochondrial function were transported to adipocytes, AMT was weakened (Fig. 6G). To further elucidate the relationship between mitochondria and AMT, we sorted EVs with high numbers or low numbers of mitochondria (Supplementary Fig. 3a). These EVs with high or low mitochondria were cocultured with adipocytes. The results revealed that vesicles carrying more mitochondria had a stronger ability to promote AMT (Fig. 6H). In summary, large vesicles from macrophages transfer mitochondria into adipocytes, which promotes AMT.

The TGF-β/PAI-1 pathway mastered the AMT

Once EVs were introduced into adipocytes, we observed significant metabolic alterations, with notable increases in both glycolytic and aerobic respiration capacities (Supplementary Fig. 3b, c), suggesting that upon stimulation by EVs, complex intracellular pathways within adipocytes underwent changes. To explore the intracellular signaling changes in adipocytes stimulated with vesicles, we conducted high-throughput bulk RNA sequencing of adipocytes treated with vesicles or left untreated. The results revealed that genes associated with fibrosis, such as *Tgfb1* and *Tgfb3*, were activated (Fig. 7A). KEGG analysis (Fig. 7B) and wiki enrichment analysis (Fig. 7C) indicated that the cytokine–cytokine receptor and TGF-β signaling pathways may be involved in vesicle-stimulated adipocytes. GSEA further revealed that ECM–receptor interactions (Fig. 7D) and the TGF-β signaling pathway (Fig. 7E) were activated in adipocytes stimulated with vesicles. Among all the differentially expressed genes, *Serpine1* (Fig. 7F) was selected as a candidate for potentially regulating vesicle-induced AMT. Therefore, we detected the plasminogen activator inhibitor-1 (PAI-1) encoded by *Serpine1* in adipocytes stimulated with vesicles, and the results revealed that PAI-1 increased once adipocytes were treated with vesicles (Fig. 7G). When we used Tm5441, an inhibitor of PAI-1[32], the AMT promoted by vesicles was weakened (Fig. 7H, I). Similarly, when we used siRNA to suppress the expression of PAI-1, the transdifferentiation of adipocytes into myofibroblasts was significantly attenuated (Fig. 7J). Overall, we concluded that the TGF-β/PAI-1 pathway is involved in the transdifferentiation of adipocytes into myofibroblasts.

Discussion

Organ fibrosis is associated with obesity. In nonalcoholic fatty liver disease, adipose tissues are closely associated with inflammation and fibrosis of the liver, and the development of fibrosis in the liver is significantly alleviated after weight loss[33]. Similarly, obesity is recognized as an independent risk factor for the development of kidney fibrosis, and bariatric surgery improves kidney outcomes in patients with chronic kidney disease[34]. The role of obesity in myocardial fibrosis is also well-established, and chronic inflammation caused by obesity promotes myocardial fibrosis[35]. In the present study, we demonstrated for the first time that patients with a higher BMI after spine surgery were more likely to suffer from FBSS, which was associated with accelerated epidural fibrosis. Similarly, in both OB/OB mice and HFD-fed mice, obesity exacerbated the formation of epidural scarring after spine operation, suggesting that adipose tissues may contribute to epidural fibrosis.

Myofibroblasts orchestrate the accumulation of extracellular matrix during wound healing and scar formation. In addition to fibroblasts, mesenchymal stem cells may also differentiate into myofibroblasts[36]. Indeed, once stimulated with EVs, MSCs may transdifferentiate into myofibroblasts (Supplementary Fig. 4). In areas where endothelial and epithelial cells are abundant, endothelial mesenchymal transformation and epithelial mesenchymal transformation also provide sources for myofibroblasts[36]. In some cases, macrophages also transdifferentiate into myofibroblasts[37]. In addition, adipocytes may be converted into myofibroblasts, thus promoting the development of fibrosis[14]. Adipocyte–myofibroblast transition (AMT) has been found in skin repair[14] and scleroderma[38], and in our study, we found that AMT also occurred in the epidural area and, at least in part, contributed to epidural fibrosis. Notably, the transdifferentiation of adipocytes into myofibroblasts still needs to be verified in a variety of diseases and different conditions[39].

As the most important immune cells in adipose tissues, macrophages play a crucial role in regulating the function of adipocytes[40]. Previous studies have suggested that the transformation of adipocytes into myofibroblasts requires a process of lipolysis, which is inseparable from the help of macrophages[14]. There is frequent mitochondrial transfer between macrophages and adipocytes[41]. Mitochondria from adipocytes could be transferred to macrophages, thereby altering their function[26]. We found that mitochondria derived from macrophages were transferred to adipocytes and changed the function of adipocytes. Nanotubes[42] and extracellular vesicles[43] were found to be common pathways for mitochondrial transport. In our study, the large extracellular vesicles carrying mitochondria from M2 macrophages promoted the adipocyte-myofibroblast transition.

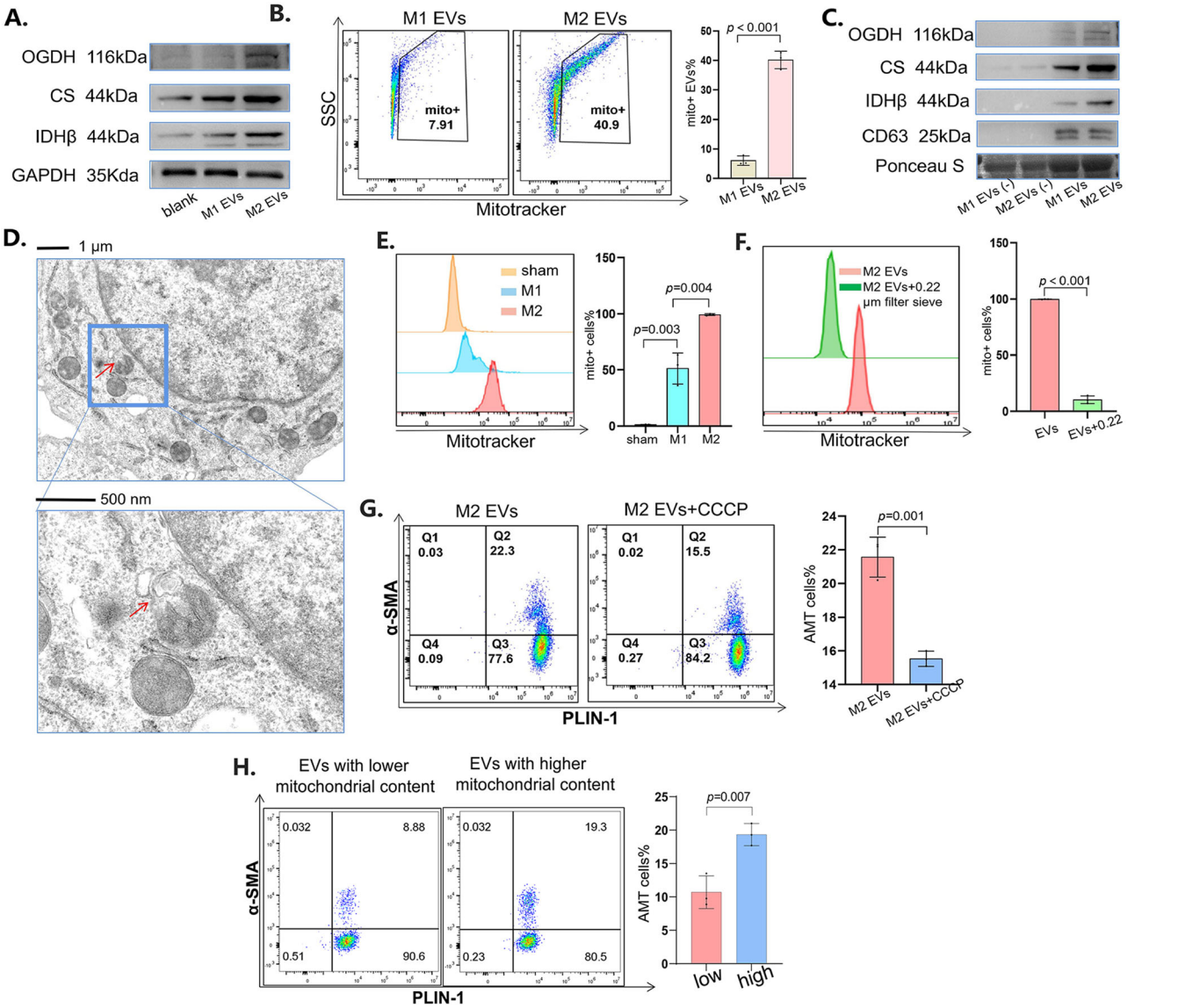

Fig. 6 | Mitochondria in large EVs promoted AMT. A Western blot analysis of OGDH, citrate synthase and IDHβ in adipocytes treated with vesicles derived from M1- or M2-type macrophages. **B** Vesicles stained with MitoTracker Red were detected via flow cytometry. On the left are typical images of flow cytometry, and on the right is the statistical graph after the experiment was repeated three times. **C** Western blot analysis of OGDH, citrate synthase and IDHβ in vesicles derived from M1- or M2-type macrophages. The supernatant after vesicle extraction was used as the control. **D** Using transmission electron microscopy, we observed that vesicles were secreted from mitochondria in M2-type macrophages. **E** After the macrophages were stained with MitoTracker Deep Red, they were cultured with adipocytes, and the portion of MitoTracker-positive adipocytes was detected via flow cytometry. On the left are typical images of flow cytometry, and on the right is the statistical graph after the experiment was repeated three times. **F** After the macrophages were stained with MitoTracker, we filtered the vesicles derived from them with a 0.22 μm sieve. After stimulation with the vesicles, the portion of MitoTracker-positive adipocytes was detected via flow cytometry. On the left are typical images of flow cytometry, and on the right is the statistical graph after the experiment was repeated three times. **G** We stimulated macrophages with CCCP and obtained vesicles derived from them. After stimulation with the vesicles, PLIN1 and α-SMA in adipocytes were detected via flow cytometry. On the left are typical images of flow cytometry, and on the right is the statistical graph after the experiment was repeated three times. **H** After adipocytes were stimulated with EVs containing different levels of mitochondria, flow cytometry was used to detect the expression levels of PLIN1 and α-SMA. All the data are presented as the mean ± Standard Error of the Mean (SEM).

Macrophage-derived mitochondria may activate specific signaling pathways in adipocytes by delivering mitochondrial DNA (mtDNA), thereby influencing the function and metabolic state of adipocytes. The promotion of AMT by macrophage-derived vesicles may involve not only the transfer of mitochondria but also the transfer of miRNAs and cytokines. Therefore, further exploration is needed to elucidate the specific mechanisms involved in these processes.

PAI-1 plays a critical role in fibrosis development, with its upregulation observed in a multitude of fibrotic conditions, including renal fibrosis[44], pulmonary fibrosis[45], and liver fibrosis[46]. Consistent with previous studies, we found that PAI-1 may also play a key role in epidural fibrosis in obese patients. Our study revealed that PAI-1 was a critical determinant facilitating the transdifferentiation of adipocytes into myofibroblasts. However, the precise mechanisms underlying PAI-1's role in this context remain to be elucidated. The reversibility of AMT upon PAI-1 inhibition offers a novel therapeutic avenue for the suppression of epidural fibrosis, suggesting that PAI-1 may serve as a clinically viable target, particularly for obese patients. In the future, extensive clinical studies and mechanistic exploration are needed to validate PAI-1 as a therapeutic target and to delineate the underlying molecular mechanisms of its role in epidural fibrosis.

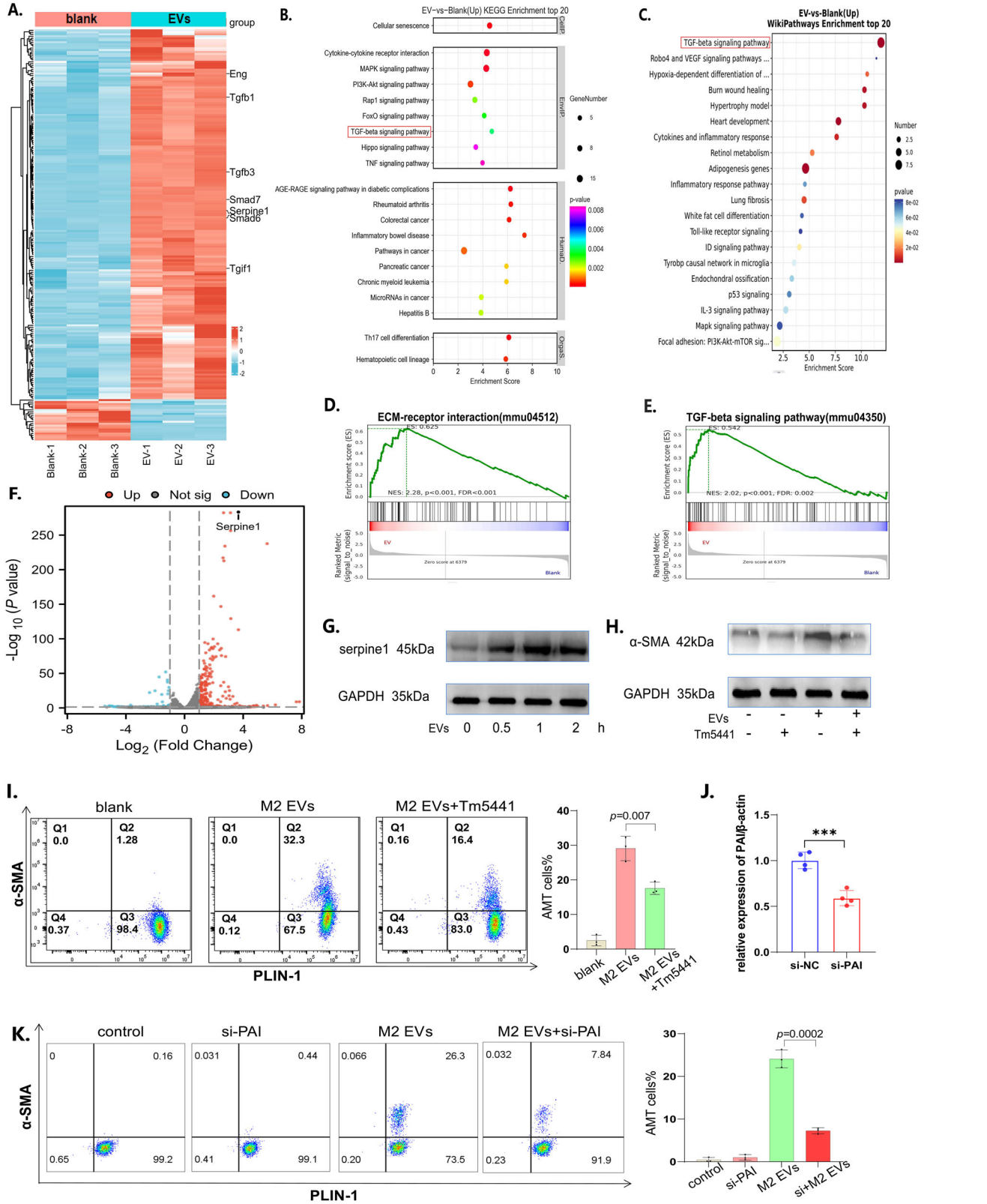

Fig. 7 | TGF-β/PAI-1 pathway mediated AMT. A The differentially expressed genes are shown as a heatmap. **B** KEGG analysis of the differentially expressed genes. **C** Wiki pathway analysis of the DEGs. **D** The ECM-receptor interaction pathway was enriched according to GSEA. **E** The TGF-β signaling pathway was enriched according to GSEA. **F** Differentially expressed genes are shown in the form of a volcano map. **G** Western blot analysis of serpine1 in adipocytes treated with vesicles at different times. **H** Western blot analysis of TGF-β in adipocytes treated with vesicles or Tm5441. **I** PLIN1 and α-SMA in adipocytes treated with vesicles or Tm5441 were detected via flow cytometry. On the left are typical images of flow cytometry, and on the right is the statistical graph after the experiment was repeated three times. **J** PAI-1 expression levels in adipocytes transfected with si-PAI were detected by qPCR. **K** PLIN1 and α-SMA expression in adipocytes was detected via flow cytometry after they were transfected with si-PAI or stimulated with EVs. All the data are presented as the mean ± Standard Error of the Mean (SEM).

Our study revealed the relationship between obesity and epidural fibrosis. Although we followed a large number of patients and obtained their preoperative and postoperative ODIs, this reflected only the extent of epidural fibrosis indirectly. MRI is the most effective method to evaluate the degree of fibrosis rather than the ODI. Since MRI is not routinely included in follow-up examinations after laminectomy, we obtained only a limited number of postoperative MR images. In addition, revision surgery is not common and is chosen only when patients suffer from severe epidural fibrosis after laminectomy. As a result, we obtained only several revision surgery samples. Finally, we do not know whether AMT is a direct transformation process or whether adipocytes first transition into mesenchymal stem cells and are later induced to become myofibroblasts. We did not investigate whether adipocytes undergoing lipolysis have a similar differentiation function as mesenchymal stem cells do. Finally, patients with a normal BMI may still develop epidural fibrosis, which may not be explained by obesity and adipocytes alone.

Methods

Clinical samples

To investigate the relationship between obesity and epidural fibrosis, we enrolled 258 patients who underwent laminectomy at the Second Affiliated Hospital of Nanjing Medical University from January 2020 to March 2021. All patients enrolled met the following criteria: (1) had low back pain and numbness in the lower limbs; (2) were positive on the straight leg elevation test; (3) magnetic resonance imaging (MRI) revealed a herniated disc at the L4–L5 level; and (4) none of the patients had cancer, autoimmune diseases, or serious infectious diseases.

We collected height and weight data from clinical patients and calculated body mass index (BMI). The Oswestry disability index (ODI) questionnaire[47] was used to obtain the degree of back pain of the patients before laminectomy and one year after surgery.

Among the patients enrolled in this investigation, 31 patients underwent MRI examination one year after surgery, and we assessed the quantity of scars in these images. Briefly, the spinal canal was subdivided into four quadrants by drawing two vertical lines from the center of the dural sac. We graded the degree of the epidural scar according to grades 0–4: grade 0, no scars; grade 1, >0 to ≤25% of the quadrants were full of scars; grade 2, >25 to ≤50% of the quadrants were full of scars; grade 3, >50 to ≤75% of the quadrants were filled with scars; and grade 4, 75–100% of the quadrants were full of scars[48].

We collected epidural scar and epidural adipose tissues removed from patients during surgery and then stored some of the tissues in liquid nitrogen and 4% paraformaldehyde for further study.

The study has been performed in accordance with the Declaration of Helsinki and approved by Ethics Committee at the Second Affiliated Hospital of Nanjing Medical University ([2019]KY056). A written informed consent form was signed by each patient.

Animals

Male C57BL/6J mice were purchased from the Animal Center of Nanjing Medical University. OB/OB (leptin KO) mice were purchased from GemPharmatech Company (Nanjing, China). To simulate diet-induced obesity, 4-week-old male mice were fed a high-fat diet (60% fat, from Xietong Pharmaceutical Company, Nanjing, China) for 16 weeks[49]. All experiments involving animal and tissue samples were performed in accordance with the guidelines and procedures approved by the Institutional Animal Care and Use Committee (IACUC) of Nanjing Medical University (IACUC-1904052).

We performed laminectomy on the mice[50]. First, the mice were intraperitoneally injected with 200 mg/kg ketamine hydrochloride (Riemser, Greifswald, Germany) and 10 mg/kg xylazine (Medistar, Ascheberg, Germany) in 100 μL of normal saline. When the mice were anesthetized, we made an incision in the skin, and the lamina from L1 to L3 was removed. For the mice in the control group, we performed a sham incision in the skin without removing the lamina. When the mice were awakened from anesthesia, they were returned to their cages.

To deplete macrophages in the mice, we injected 200 μL of clodronate liposomes (5 mg/mL, Yeasen, Shanghai, China) intraperitoneally into the mice 24 h before laminectomy.

Before the mice were sacrificed via cervical dislocation, they were injected with 200 mg/kg ketamine hydrochloride and 10 mg/kg xylazine in 100 μL of normal saline.

Cell culture

The macrophages were derived from bone marrow. Briefly, we acquired tibias and femurs from mice after they were sacrificed via cervical dislocation, and we rinsed the bone marrow with cold phosphate-buffered saline (PBS). After centrifugation at 4°C and 500 × g for 5 min in red blood cell lysis buffer (Thermo Fisher Scientific, MA, USA), cell precipitates were obtained. Subsequently, the cells were washed twice with PBS and resuspended at a concentration of 2 × 10^6 cells/mL in Dulbecco's modified Eagle medium (DMEM) (Sigma, Shanghai, China, D5030) supplemented with 10% fetal bovine serum (Gibco, MA, USA), 100 U/mL penicillin, and 0.1 mg/mL streptomycin, and most of the cells were monocytes. To induce monocytes to differentiate into M1- or M2-type macrophages, we used 10 ng/mL granulocyte–macrophage colony-stimulating factor (GM-CSF; Biolegend, CA, USA; Cat# 576308) or macrophage–colony-stimulating factor (M-CSF; Biolegend, CA, USA; Cat# 576408) to stimulate the cells. Following 7 days of stimulation, mature macrophages were obtained.

Adipocytes were harvested from adipose tissues. Adipose tissues from the groin of the mice were excised and immersed in cold PBS. The adipose tissues were minced and digested with collagenase 1 (Sigma, Shanghai, China) for 60 min. The cells were subsequently filtered through a 70 μm cell sieve and cultured in petri dishes with DMEM. After 3 passages, we obtained pure precursor adipocytes. When the cells in the dish reached 80% confluence, they were transferred to a 24-well plate for differentiation. When the precursor adipocytes had allowed for 2 days, we added high-glucose DMEM supplemented with IBMX (250 μM) (Sigma, Shanghai, China), insulin (0.5 μg/ml) (Sigma, Shanghai, China), and dexamethasone (1 μM) (Sigma, Shanghai, China) instead of normal DMEM. After 5 days, the medium was replaced with high-glucose DMEM containing insulin (0.5 μg/ml) for further culture. Mature adipocytes were available at 14 days after induction.

To obtain mesenchymal stem cells[51], the bone marrow cells were plated in a T75 flask and incubated at 37°C in a humidified atmosphere with 5% CO_2. After 24 h, the nonadherent cells were removed by washing with PBS, leaving only the adherent cell population. These cells were maintained until they reached approximately 80% confluence. The cells were subsequently passaged three times to enrich for the MSC population. After the third passage, a relatively pure population of BM-MSCs was obtained and used for further experiments.

Histological analysis

The mice were sacrificed at 30 days after laminectomy to obtain spinal tissues from L1 to L3. Epidural fat tissues were obtained from patients during laminectomy. The tissues were fixed in 4% paraformaldehyde and embedded in paraffin.

To observe the association between adipocytes and fibrosis, we used immunofluorescence in mouse spinal tissues and human adipose tissue samples. Briefly, the embedded tissues were cut into 4 μm thick sections and incubated with anti-α-SMA (1:100, mouse monoclonal, ab7817, Abcam) and anti-PLIN1 (1:100, rabbit polyclonal, ab3526, Abcam) at 4°C for 24 h. Then, the slides were incubated with goat anti-rabbit IgG (1:100, Alexa Fluor® 488, ab150077, Abcam) and goat anti-mouse IgG (1:100, Alexa Fluor® 594, ab150120, Abcam) for 2 h at 27°C and then observed under the fluorescence microscope.

To investigate the relationship between macrophages and adipocytes, we cut the spinal tissues from the mice into 4 μm thick sections and incubated them with anti-PLIN1 (1:100, rabbit polyclonal, ab3526, Abcam) and anti-F4/80 (1:100, rat monoclonal, ab6640, Abcam) at 4°C for 24 h.

Following this, the slides were incubated with goat anti-rabbit IgG (1:100, Alexa Fluor® 488, ab150077, Abcam) and goat anti-rat IgG (1:100, Alexa Fluor® 594, ab150160, Abcam) for 2 h at 27°C and then observed under a fluorescence microscope.

To observe cell morphology and inflammatory cell infiltration in the scar tissues, hematoxylin–eosin (H&E) staining (abs9217, Absin) was used in mouse spinal tissues and adipose tissues from patients. The sections of the tissues were fixed in 95% ethanol for 2 min and washed with PBS for 5 min. The sections were subsequently placed sequentially in hematoxylin solution for 3 min and eosin solution for 3 min. We washed the sections with PBS before each change in dye solution, and the slides were imaged via a microscope.

Masson's trichrome solution (abs9347, Absin) was used to label the collagenous fibers in the spinal tissues of the mice. We placed the sections sequentially into Bouin's solution for 30 min, Weigert's hematoxylin solution for 10 min, Biebrich scarlet solution for 10 min, phosphotungstic acid-phospholimbic acid solution for 15 min, and aniline blue solution for 2 min. Finally, the sections were rinsed in a 1% acetic acid bath, treated with alcohol, and permeabilized with xylene. Finally, the slides were imaged with a microscope.

To demonstrate the degree of epidural fibrosis, immunohistochemical staining was performed on the spinal tissues of the mice. In brief, the embedded tissues were cut into 4 μm thick sections and incubated with anti-α-SMA (1:100, mouse monoclonal, ab7817, Abcam). Then, the slides were incubated with goat anti-mouse IgG (1:100, HRP, ab6789, Abcam) for 2 h at 27°C and observed with a microscope.

Western blot analysis

To detect proteins in the tissues, we performed western blot analysis. Briefly, the tissues were cut into pieces and lysed in radioimmunoprecipitation assay buffer supplemented with 1 mM phenylmethanesulfonyl fluoride. Loading buffer (5×) was added to the lysis buffer. Equal volumes of sample were loaded to a 10% sodium dodecyl sulfate–polyacrylamide gel. The proteins were subsequently separated via electrophoresis and transferred to polyvinylidene fluoride membranes. The membranes were immersed in 5% bovine serum albumin at 27°C for 1 hour to avoid nonspecific binding of the antibody to the antigen. Then, we rinsed the membranes in PBS containing Tween 3 times and incubated them with anti-ACSL1 (1:1000, rabbit polyclonal, ab189939, Abcam), anti-DGAT1 (1:1000, rabbit monoclonal, ab179711, Abcam), anti-fibronectin (1:1000, rabbit monoclonal, ab268020, Abcam), anti-α-SMA (1:1000, rabbit monoclonal, ab124964, Abcam) and anti-β-Actin (1:1000, rabbit polyclonal, ab8227, Abcam) secondary antibodies at 4°C overnight. Finally, the membranes were incubated with goat anti-rabbit IgG (1:5000, HRP, ab6721, Abcam). The proteins in the membranes were detected with enhanced chemiluminescence high-signal reagents (36208ES60, Yeasen). β-Actin was used to normalize the expression of all the proteins.

Similarly, the proteins of the adipocytes were also extracted in radioimmunoprecipitation assay buffer and measured by western blotting. As described previously, the membranes were incubated with anti-PLIN1 (1:1000, rabbit polyclonal, ab3526, Abcam), anti-fibronectin (1:1000, rabbit monoclonal, 1:1000, ab268020, Abcam), anti-α-SMA (1:1000, rabbit monoclonal, ab124964, Abcam), anti-β-actin (1:1000, rabbit polyclonal, ab8227, Abcam), anti-OGDH (1:1000, rabbit monoclonal, ab307370, Abcam), anti-citrate synthase (1:1000, rabbit polyclonal, ab129095, Abcam), anti-IDHβ (1:1000, rabbit polyclonal, ab131263, Abcam), anti-PAI-1 (1:1000, rabbit monoclonal, ab182973, Abcam) and anti-GAPDH (1:1000, rabbit polyclonal, ab9485, Abcam) antibodies. The expression of all proteins was normalized to that of β-actin or GAPDH.

For the proteins in the extracellular vesicles, we directly mixed 5× loading buffer with the vesicle mixture. The proteins in the membranes were incubated with anti-CD81 (1:1000, rabbit monoclonal, 1:1000, ab109201, Abcam), anti-CD63 (1:1000, rabbit monoclonal, 1:1000, ab217345, Abcam), anti-flotillin (1:1000, rabbit monoclonal, ab133497, Abcam), anti-OGDH (1:1000, rabbit monoclonal, ab307370, Abcam), anti-citrate synthase (1:1000, rabbit polyclonal, ab129095, Abcam), and anti-IDHβ (1:1000, rabbit polyclonal, ab131263, Abcam) antibodies. The expression of all proteins was normalized by PonceauS staining.

Oil Red O staining

To observe the formation of lipid droplets in adipocytes, Oil Red O staining was used. Briefly, the cells were washed with PBS three times and fixed with 4% paraformaldehyde for 15 min. The cells were subsequently incubated with Oil Red O solution (Cat# MAK194; Sigma–Aldrich) for 15 min. Finally, the cells were washed with PBS to remove the residual Oil Red O solution and observed under a microscope.

Flow cytometry

The tissue samples were minced and digested with collagenase for 30 min, the mixture was passed through a 100 μm sieve to obtain single-cell suspensions. The suspensions were incubated with anti-PLIN1 (1:100, rabbit polyclonal, ab3526, Abcam) and anti-α-SMA (1:100, mouse monoclonal, ab7817, Abcam) antibodies for 2 h at 27°C. The suspensions were subsequently washed with PBS 3 times and incubated with goat anti-rabbit IgG (1:100, Alexa Fluor® 750, ab175735, Abcam) and goat anti-mouse IgG (1:100, FITC, ab6785, Abcam) for 1 hour at 27°C.

The cells were obtained with pancreatic enzymes, centrifuged and resuspended into single-cell suspensions. The cells were incubated with anti-PLIN1 (1:100, rabbit polyclonal, ab3526, Abcam), anti-α-SMA (1:100, mouse monoclonal, ab7817, Abcam) for 2 h at 27°C, MitoTracker Red (100 nM, 40741ES50, Yeasen), or MitoTracker Deep Red (100 nM, 40743ES50, Yeasen) for 30 min at 27°C. The cells were subsequently incubated with goat anti-rabbit IgG (1:100, Alexa Fluor® 488, ab150077, Abcam), goat anti-mouse IgG (1:100, APC-Cy7, ab130785, Abcam) or goat anti-mouse IgG (1:100, Alexa Fluor® 750, A21037, Thermo Fisher) for 1 hour at 27°C. Anti-CD34 (1:100, rabbit monoclonal, ab81289, Abcam), anti-CD45 (1:100, rabbit monoclonal, ab317446, Abcam), anti-CD73 (1:100, rabbit multiclonal, ab317462, Abcam), anti-CD105 (1:100, rabbit monoclonal, ab221675, Abcam), and anti-CD90 (1:100, rabbit monoclonal, ab307736, Abcam) and the corresponding secondary fluorescence antibodies were used to identify mesenchymal stem cells via flow cytometry. The data were collected on a Beckman CytoFLEX Cytometer and analyzed via FlowJo v10 software.

Adipocyte plasmid transfection

The method used for plasmid transfection of adipocytes has been described previously[52]. Briefly, murine 3T3-L1 preadipocytes were differentiated into fully lipid-laden adipocytes via a standard induction cocktail of 3-isobutyl-1-methylxanthine/IBMX, dexamethasone, and insulin. Adipocytes were seeded in 6-well plates at a density of 1×10^5 cells per well in complete culture medium and incubated overnight until they reached approximately 50–70% confluence. To knock down serpine1 (PAI), the cells were transfected with a siRNA plasmid (BIOG, China) via Lipofectamine RNAi^{MAX} transfection reagent (Invitrogen) according to the manufacturer's instructions. The cells were incubated further 24 h to allow for gene silencing. The forward sequence of si-PAI is GGA GAU GGU UAU AGA CCG ATT, and the reverse sequence is UCG GUC UAU AAC CAU CUC CTT.

Cell fluorescence

To observe the lipid droplets in adipocytes and the extracellular matrix secreted by adipocytes, we washed the cells three times with PBS and fixed them with 4% paraformaldehyde. Then, the adipocytes were incubated with an anti-α-SMA antibody (1:100, mouse monoclonal, ab7817, Abcam) for 1 hour at 27°C. The cells were subsequently incubated with goat anti-mouse IgG (1:100, Alexa Fluor® 594, ab150120, Abcam) and BODIPY 493/503 (1 μM, Cat# 790389, Sigma–Aldrich) for 1 hour. Images of these cells were captured under a fluorescence microscope.

Seahorse metabolic assay

For the Seahorse XF assay to measure cellular respiration and glycolysis, the cells were seeded in a Seahorse XF96 cell culture microplate at a density of 1×10^4 cells per well. On the day of the assay, the medium was aspirated, and the cells were washed with 1 mL of Seahorse XF Base Medium supplemented with 1 mM pyruvate, 10 mM glucose, and 2 mM glutamine. Then the cells were incubated with 180 μL of supplemented XF Base Medium for 1 hour at 37°C without CO2. The Seahorse XF96 cartridge was hydrated overnight in XF Calibrant Solution. Following the equilibration period, the microplate was loaded into the Seahorse XF Analyzer, and the oxygen consumption rate (OCR) and extracellular acidification rate (ECAR) were measured at baseline and after sequential injections of oligomycin, FCCP, and rotenone/antimycin A for the Mito Stress Test or glucose, oligomycin, and 2-deoxyglucose for the Glycolysis Stress Test.

Exosome isolation and identification

When the macrophages matured, the original medium was replaced with exosome-free fetal bovine serum. After 24 h, the medium was collected and centrifuged at 500×g at 4°C for 10 min. The precipitate of the cells was discarded, and the supernatant was centrifuged at 2000×g for 15 min. Then, the precipitate of the dead cells was discarded. The supernatant was collected and centrifuged at 10,000 ×g for 30 min. Finally, the precipitate of cell debris was discarded, and the supernatant was centrifuged at 100,000 ×g at 4°C for 60 min. The supernatant was then discarded, and the exosomes were suspended in sterile PBS and stored at -80°C.

The size distribution of the exosomes was explored via nanoparticle tracking analysis (NTA). Transmission electron microscopy (TEM) was used to observe the exosomes. Specific protein markers for the exosomes were detected via western blotting.

Quantitative polymerase chain reaction

Total RNA was extracted from adipocytes stimulated with M2-EVs for 24 h via a TRIzol reagent kit according to the manufacturer's protocol. The extracted RNA was then reverse-transcribed into cDNA via a commercially available kit as directed by the supplier's instructions. Quantitative real-time PCR (qPCR) was performed on a StepOnePlus Real-Time PCR System to assess PAI mRNA expression. The sequences of primers used for PAI were (forward) 5′-AGG AGA UGG UUA UAG ACC GAT T-3′ and (reverse) 5′-AAC CAG UAA CCA UCU CCA ATT-3′. The primer sequences for the housekeeping gene β-actin were (forward) 5′-GCA CCA CAG ACG CGA TCT T-3′ and (reverse) 5′-ACC TCT GAA AAG TCC ACT TGC-3′. β-Actin was utilized as the internal control. Relative mRNA levels of PAI and β-actin were calculated via the $2^{-\Delta\Delta Ct}$ method.

High-throughput mRNA sequencing and proteomics analysis

For high-throughput mRNA sequencing, adipocytes were treated with exosomes derived from M2-type macrophages for 1 hour, while the control group remained untreated. Total mRNA was subsequently extracted with TRIzol according to the manufacturer's instructions. After mRNA quality and integrity were measured, the mRNA was quantified and subjected to stranded RNA sequencing in collaboration with OE Biotech Company (Shanghai, China). RNA sequencing was performed via an Illumina NovaSeq 6000 sequencer. The genes whose P value was less than 0.05 and whose fold change was greater than 2 or less than 0.5 were defined as DEGs (differentially expressed genes). We subsequently carried out Kyoto Encyclopedia of Genes and Genomes (KEGG) analysis, Wiki pathway analysis and gene set enrichment analysis (GSEA) on the DEGs and used R (v 3.2.0) to construct volcano diagrams, heatmaps and enrichment analysis diagrams.

For proteomics, the clinical specimens from 3 patients were ground into powder, which was then ultrasonically cracked. The same amount of protein was taken from each sample for enzymolysis, and the peptide segment was obtained after enzymolysis. The peptides were labeled according to the TMT kit instructions (Jingjie Biotech Company, Shanghai, China). The peptides were then analyzed via liquid chromatography–mass spectrometry. In all three groups, proteins with a fold change greater than 1.2 or less than 0.8 were defined as differentially expressed proteins. Heatmaps of these differentially expressed proteins were generated. To gain deeper insight into the biological functions and pathways associated with the differentially expressed proteins, we conducted functional enrichment analysis using Kyoto Encyclopedia of Genes and Genomes (KEGG) and Gene Ontology (GO) analyses. KEGG pathway analysis identified the biological pathways that are significantly enriched among the differentially expressed proteins, providing a comprehensive view of the molecular interaction and reaction networks. Meanwhile, GO analysis categorized the proteins based on their involvement in cellular components, molecular functions, and biological processes, thereby offering a detailed understanding of the specific roles and potential implications of these proteins within the cellular context. The mass spectrometry proteomics data have been deposited to the ProteomeXchange Consortium (https://proteomecentral.proteomexchange.org) via the iProXpartner repository with the dataset identifier PXD059035.

Elisa

To calculate specific collagen levels in the epidural areas of the mice, the spinal tissues were cut into pieces and centrifuged at 4°C and 10,000 × g for 10 min with lysis buffer. The supernatant was collected, and the collagen I content was measured with a collagen I ELISA kit (Beijing Long Tian Technology, Beijing, China).

Magnetic resonance imaging

MRI was performed 1 year post spine operation. The patients were prepared for the examination according to the standard protocol. Prior to the MRI, all metallic objects and electronic devices were removed from the patient to ensure safety and image quality. The patients were instructed to lie in a supine position on the MRI table. For comfort and to minimize motion artifacts, cushions and straps were used to secure the patient. Anesthesia was not required; however, if necessary, sedation was administered under the supervision of an anesthesiologist. The MRI scans were acquired using a 3.0 Tesla clinical MRI system. A T2-weighted imaging (T2WI) sequence was employed, with the following parameters: time of repetition (TR) 4000 ms, echo time (TE) 90 ms, slice thickness 5 mm, interslice gap 1 mm, and matrix size 256×256. The field of view (FOV) was adjusted to cover the region of interest, which in this case was the lumbar spine (L1-L5). The total scan time per sequence was approximately 8 min. Additional sequences, such as T1-weighted imaging (T1WI) and diffusion-weighted imaging (DWI), were also performed to provide complementary information about the tissue characteristics. The epidural scar area, if present, was measured using the software's measurement tools. All measurements were conducted by two independent radiologists, and any discrepancies were resolved through consensus. The data were then analyzed to assess the extent of the scar formation and its impact on the spinal canal and nerve roots.

Statistical analysis

All the data are presented as the mean ± Standard Error of the Mean (SEM). Statistical analyses were conducted via Prism (GraphPad) software. Unpaired Student's t test and one-way ANOVA were used to determine statistically significant differences between groups.

Data availability

The datasets are available from the corresponding author upon reasonable request. The bulk RNA-Seq data in the project have been submitted to Sequence Read Archive with the accession number of PRJNA1158572.

Received: 11 May 2024; Accepted: 24 December 2024;
Published online: 30 December 2024

References

1. Hua, F. et al. Substance P promotes epidural fibrosis via induction of type 2 macrophages. *Neural Regen. Res.* **18**, 2252–2259 (2023).

2. Katz, J. N., Zimmerman, Z. E., Mass, H. & Makhni, M. C. Diagnosis and management of lumbar spinal stenosis: a review. *JAMA* **327**, 1688–1699 (2022).
3. Alizadeh, R. & Sharifzadeh, S. R. Pathogenesis, etiology and treatment of failed back surgery syndrome. *Neurochirurgie* **68**, 426–431 (2022).
4. Rabb, C. H. Failed back syndrome and epidural fibrosis. *Spine J.* **10**, 454–455 (2010).
5. Parenteau, C. S., Lau, E. C., Campbell, I. C. & Courtney, A. Prevalence of spine degeneration diagnosis by type, age, gender, and obesity using Medicare data. *Sci. Rep.* **11**, 5389 (2021).
6. Sachs, S. et al. GIP receptor agonism improves dyslipidemia and atherosclerosis independently of body weight loss in preclinical mouse model for cardio-metabolic disease. *Cardiovasc. Diabetol.* **22**, 217 (2023).
7. Lawrence, S. et al. Anatomy of the lumbar interspinous ligament: findings relevant to epidural insertion using loss of resistance. *Reg. Anesth. Pain Med.* **46**, 1085–1090 (2021).
8. Shah, S. et al. Prx1 + and Hic1+ mesenchymal progenitors are present within the epidural fat and dura mater and participate in dural injury repair. *Stem Cells Transl. Med.* **11**, 200–212 (2022).
9. Dou, X. et al. Fibrotic and inflammatory characteristics of epidural fat adjacent to the ossification area in patients with ossification of the ligament flavum. *JOR Spine* **5**, e1229 (2022).
10. Sabaratnam, R., Hansen, D. R. & Svenningsen, P. White adipose tissue mitochondrial bioenergetics in metabolic diseases. *Rev. Endocr. Metab. Disord*. **24**, 1121–1133 (2023).
11. Jones, J. E. C. et al. The adipocyte acquires a fibroblast-like transcriptional signature in response to a high fat diet. *Sci. Rep.* **10**, 2380 (2020).
12. Kruglikov, I. L., Zhang, Z. & Scherer, P. E. Phenotypical conversions of dermal adipocytes as pathophysiological steps in inflammatory cutaneous disorders. *Int. J. Mol. Sci.* **23**, 3828 (2022).
13. Martins, V. et al. FIZZ1-induced myofibroblast transdifferentiation from adipocytes and its potential role in dermal fibrosis and lipoatrophy. *Am. J. Pathol.* **185**, 2768–2776 (2015).
14. Shook, B. A. et al. Dermal adipocyte lipolysis and myofibroblast conversion are required for efficient skin repair. *Cell Stem Cell* **26**, 880–895.e886 (2020).
15. Ruf, B. et al. Tumor-associated macrophages trigger MAIT cell dysfunction at the HCC invasive margin. *Cell* **186**, 3686–3705.e3632 (2023).
16. Strizova, Z. et al. M1/M2 macrophages and their overlaps—myth or reality? *Clin. Sci.* **137**, 1067–1093 (2023).
17. Liang, W. et al. Mitochondria are secreted in extracellular vesicles when lysosomal function is impaired. *Nat. Commun.* **14**, 5031 (2023).
18. Kalluri, R. & LeBleu, V. S. The biology, function, and biomedical applications of exosomes. *Science.* **367**, eaau6977 (2020).
19. van der Vlist, M. et al. Macrophages transfer mitochondria to sensory neurons to resolve inflammatory pain. *Neuron* **110**, 613–626.e619 (2022).
20. Nunnari, J. & Suomalainen, A. Mitochondria: in sickness and in health. *Cell* **148**, 1145–1159 (2012).
21. Al Amir Dache, Z. & Thierry, A. R. Mitochondria-derived cell-to-cell communication. *Cell Rep.* **42**, 112728 (2023).
22. Ji, L. et al. AKAP1 deficiency attenuates diet-induced obesity and insulin resistance by promoting fatty acid oxidation and thermogenesis in brown adipocytes. *Adv. Sci.* **8**, 2002794 (2021).
23. Chitraju, C. et al. Triglyceride synthesis by DGAT1 protects adipocytes from lipid-induced ER stress during lipolysis. *Cell Metab.* **26**, 407–418.e403 (2017).
24. Wang, S. et al. PPAR-γ integrates obesity and adipocyte clock through epigenetic regulation of Bmal1. *Theranostics* **12**, 1589–1606 (2022).
25. Jaitin, D. A. et al. Lipid-associated macrophages control metabolic homeostasis in a Trem2-dependent manner. *Cell* **178**, 686–698.e614 (2019).
26. Borcherding, N. et al. Dietary lipids inhibit mitochondria transfer to macrophages to divert adipocyte-derived mitochondria into the blood. *Cell Metab.* **34**, 1499–1513.e1498 (2022).
27. Xie, M. et al. FGF19/FGFR4-mediated elevation of ETV4 facilitates hepatocellular carcinoma metastasis by upregulating PD-L1 and CCL2. *J. Hepatol.* **79**, 109–125 (2023).
28. Liu, Y. et al. Fine particulate matter (PM2.5) induces inhibitory memory alveolar macrophages through the AhR/IL-33 pathway. *Cell. Immunol.* **386**, 104694 (2023).
29. Wang, Y. et al. Macrophage-derived extracellular vesicles: diverse mediators of pathology and therapeutics in multiple diseases. *Cell Death Dis.* **11**, 924 (2020).
30. Gan, L. et al. Ischemic heart-derived small extracellular vesicles impair adipocyte function. *Circ. Res.* **130**, 48–66 (2022).
31. Wu, C. et al. Iron induces B cell pyroptosis through Tom20-Bax-caspase-gasdermin E signaling to promote inflammation post-spinal cord injury. *J. Neuroinflammation* **20**, 171 (2023).
32. Catarinella, G. et al. SerpinE1 drives a cell-autonomous pathogenic signaling in Hutchinson-Gilford progeria syndrome. *Cell Death Dis.* **13**, 737 (2022).
33. Younossi, Z. M., Corey, K. E. & Lim, J. K. AGA clinical practice update on lifestyle modification using diet and exercise to achieve weight loss in the management of nonalcoholic fatty liver disease: expert review. *Gastroenterology* **160**, 912–918 (2021).
34. Sandino, J., Martįn-Taboada, M., Medina-Gómez, G., Vila-Bedmar, R. & Morales, E. Novel insights in the physiopathology and management of obesity-related kidney disease. *Nutrients* **14**, 3937 (2022).
35. Ren, J., Wu, N. N., Wang, S., Sowers, J. R. & Zhang, Y. Obesity cardiomyopathy: evidence, mechanisms, and therapeutic implications. *Physiol. Rev.* **101**, 1745–1807 (2021).
36. LeBleu, V. S. et al. Origin and function of myofibroblasts in kidney fibrosis. *Nat. Med.* **19**, 1047–1053 (2013).
37. Tang, P. M., Nikolic-Paterson, D. J. & Lan, H. Y. Macrophages: versatile players in renal inflammation and fibrosis. *Nat. Rev. Nephrol.* **15**, 144–158 (2019).
38. Kruglikov, I. L. Interfacial adipose tissue in systemic sclerosis. *Curr. Rheumatol. Rep.* **19**, 4 (2017).
39. Kalgudde Gopal, S. et al. Wound infiltrating adipocytes are not myofibroblasts. *Nat. Commun.* **14**, 3020 (2023).
40. Joffin, N. et al. Adipose tissue macrophages exert systemic metabolic control by manipulating local iron concentrations. *Nat. Metab.* **4**, 1474–1494 (2022).
41. Brestoff, J. R. et al. Intercellular mitochondria transfer to macrophages regulates white adipose tissue homeostasis and is impaired in obesity. *Cell Metab.* **33**, 270–282.e278 (2021).
42. Saha, T. et al. Intercellular nanotubes mediate mitochondrial trafficking between cancer and immune cells. *Nat. Nanotechnol.* **17**, 98–106 (2022).
43. Rosina, M. et al. Ejection of damaged mitochondria and their removal by macrophages ensure efficient thermogenesis in brown adipose tissue. *Cell Metab.* **34**, 533–548.e512 (2022).
44. Chen, B. H., Lu, X. Q., Liang, X. H. & Wang, P. Serpin E1 mediates the induction of renal tubular degeneration and premature senescence upon diabetic insult. *Sci. Rep.* **13**, 16210 (2023).
45. Chung, E. J. et al. Truncated plasminogen activator inhibitor-1 protein protects from pulmonary fibrosis mediated by irradiation in a murine model. *Int. J. Radiat. Oncol. Biol. Phys.* **94**, 1163–1172 (2016).
46. Verrijken, A. et al. Prothrombotic factors in histologically proven nonalcoholic fatty liver disease and nonalcoholic steatohepatitis. *Hepatology* **59**, 121–129 (2014).

47. Austevoll, I. M. et al. Decompression with or without fusion in degenerative lumbar spondylolisthesis. *N. Engl. J. Med.* **385**, 526–538 (2021).
48. Ding, Q. et al. The preventive effect of decorin on epidural fibrosis and epidural adhesions after laminectomy. *Front. Pharm.* **12**, 774316 (2021).
49. Emont, M. P. et al. A single-cell atlas of human and mouse white adipose tissue. *Nature* **603**, 926–933 (2022).
50. Jin, Z. et al. Neutrophil extracellular traps promote scar formation in post-epidural fibrosis. *NPJ Regen. Med.* **5**, 19 (2020).
51. Soleimani, M. & Nadri, S. A protocol for isolation and culture of mesenchymal stem cells from mouse bone marrow. *Nat. Protoc.* **4**, 102–106 (2009).
52. Paneru, B. D. et al. Myeloid-derived miR-6236 potentiates adipocyte insulin signaling and prevents hyperglycemia during obesity. *Nat. Commun.* **15**, 5394 (2024).

Acknowledgements

This study was supported by the National Natural Science Foundation of China (82172486, 82171738), the Jiangsu Provincial Commission of Health and Family Planning, the “Six One” Project of Jiangsu Province LGY2016018 and the Jiangsu Provincial Personnel Department “the Great of Six Talented Man Peak” Project WSW-040.

Author contributions

F.H. performed the experiments, analyzed the data, and wrote the paper. J.S., M.S., R.M., and Z.S. performed the experiments and analyzed the data. J.L. and M.Z. conceived and designed the experiments, analyzed the data, and wrote the paper.

Competing interests

The authors declare no competing interests.

Additional information

Supplementary information The online version contains supplementary material available at https://doi.org/10.1038/s41536-024-00388-6.

Correspondence and requests for materials should be addressed to Jun Liu or Mingshun Zhang.